Microchimica Acta
https://doi.org/10.1007/s00604-019-3283-2

ORIGINAL PAPER

Determination of Alzheimer biomarker DNA by using an electrode modified with in-situ precipitated molybdophosphate catalyzed by alkaline phosphatase-encapsulated DNA hydrogel and target recycling amplification

Xiaoyu Hua[1] · Xingxing Zhou[1] · Shijing Guo[1] · Ting Zheng[1] · Ruo Yuan[1] · Wenju Xu[1]

Received: 30 September 2018 / Accepted: 24 January 2019

Abstract

An electrochemical biosensor is described for highly sensitive determination of tDNA, an Alzheimer's disease (AD)-related biomarker. Electroactive molybdophosphate anions were precipitated in-situ on a glassy carbon electrode (GCE) via catalytic hydrolysis by alkaline phosphatase (ALP). This is followed by recycling amplification of tDNA. Four DNA strands (referred to as S1, S2, S3 and S4) were designed to assemble X-shape DNA (X-DNA) building blocks. These were further extended into four directions under the action of DNA polymerase. The resultant two X-DNA motifs were polymerize. Simultaneously, ALP is encapsulated into a hydrogels network to obtain a porous material of type ALP@DNAhg. The GCE was modified with reduced graphene oxide functionalized with gold nanoparticles (Au@rGO). If ALP@DNAhg are captured via strand displacement, tDNA recycling assembly for signal amplification is initiated. This results in the immobilization of large amounts of ALP. On introduction of pyrophosphate and molybdate (MoO_4^{2-}), ALP will catalyze the hydrolysis of pyrophosphate to produce phosphate. It will react with molybdate to form redox active phosphomolybdate anions ($PMo_{12}O_{40}^{3-}$). Its amperometrical signal depends on the concentration of tDNA in the 1.0×10^{-2} to 1.0×10^{4} pM concentration range, and the detection limit is 3.4×10^{-3} pM.

Keywords Label-free detection · Electrochemical biosensor · AuNP-functionalized reduced graphene oxide · X-shape DNA building block · Pyrophosphate · Molybdate · In-situ precipitation · Networked DNA structure · Enzymatic catalysis · Redox active phosphomolybdate anions

Introduction

As well known, the electroactive substance as redox electron mediator is a key component in constructing electrochemical detection system [1–3]. To date, many interesting progresses have focused on the direct electron transfer of some redox proteins such as hemin/G-quarduplex and hemoglobin [4–7], and metal nanomaterials [8–10]. More importantly, electroactive mediators were in situ homogeneously generated through chemical combination [4]. As one of polyoxometalatcs anions, Keggin-structure α-molybdophosphate anion ($PMo_{12}O_{40}^{3-}$) can undergo reversible multi-electron oxidation and reduction processes. In addition, multi-pair of electrochemical redox peaks of $PMo_{12}O_{40}^{3-}$ can be directly obtained at certain solution condition [11, 12]. It is very interesting and potential to use $PMo_{12}O_{40}^{3-}$ as electron mediator in label-free biosensors, enabling convenient, rapid and cost-effective detection of protein, microRNA, DNA, enzymes et al. [13–19]. For example, phosphate groups in hydroxyapatite nanoparticles or DNA strand backbones directly reacted with MoO_4^{2-} to precipitate $PMo_{12}O_{40}^{3-}$ for electrochemical signal readout [13–16]. Moreover, two electrochemical biosensors were developed based on $PMo_{12}O_{40}^{3-}$ as redox mediator, which was obtained by the reaction of MoO_4^{2-} with PO_4^{3-}. Especially, PO_4^{3-} was generated through the pyrophosphate ($P_2O_7^{4-}$) hydrolysis catalyzed by pyrophosphatase and the 1-naphthyl

Electronic supplementary material The online version of this article (https://doi.org/10.1007/s00604-019-3283-2) contains supplementary material, which is available to authorized users.

✉ Wenju Xu
xwju@swu.edu.cn

[1] Key Laboratory of Luminescent and Real-Time Analytical Chemistry, Ministry of Education, School of Chemistry and Chemical Engineering, Southwest University, Chongqing 400715, People's Republic of China

Published online: 04 February 2019

phosphate (NPP) hydrolysis catalyzed by alkaline phosphatase (ALP), respectively [17, 18]. These strategies will provide a new way to construct simple and cost-effective biosensors. Nevertheless, it is necessary to improve the immobilization of enzymes in electrode surface for the long-term stability of precipitated $PMo_{12}O_{40}^{3-}$.

Because of high payload capacity, easy preparation, mechanical flexibility and stability, DNA-based hydrogels (DNAhg) are attractive biomaterial candidates to encapsulate bioactive molecules, control drug/enzymes delivery and release [20], activate cascaded biocatalysis [21], and fabricate biosensors [22]. Based on a particular protocol, numerous DNA building blocks can be elaborately designed, such as branched double-stranded, X-shaped or/and Y-shaped DNA. Through different affinity interaction or DNA hybridization, diverse DNAhg with networked structure and good porosity can be assembled easily and rapidly upon the catalysis of DNA terminal transferase (TdT) [23]. In the DNAhg scaffold, enzymes or metal nanoparticles can be stably enwrapped, and their catalytic activity would be maintained like before encapsulation. For example, a horseradish peroxidase-encapsulated DNAhg was developed for dual-amplified colorimetric detection of ochratoxin A [24]. Li's group used a novel DNAhg to entrap Au nanoparticle for the detection of H_2O_2 and glucose [25]. A simple method was reported to assemble DNAhg for HRP immobilization, in which the enwrapped HRP retained stable catalytic activities without any losing [26]. As such, versatile DNAhg as the matrices showed great flexibility and capability to preserve the biological activity of encapsulated biomolecules [23, 27].

Inspired by these observations, an electrochemical biosensor was developed for the detection of target DNA (tDNA), an important Alzheimer's disease (AD)-related biomarker [28]. The detection route was based on ALP-encapsulated DNA hydrogels (ALP@DNAhg) to catalyze in situ precipitation of redox active $PMo_{12}O_{40}^{3-}$ anions and tDNA recycling amplification. Here, ALP@DNAhg was constructed via the extension and polymerization of a X-shape DNA building block (X-DNA), along with the simultaneous enwrapping of ALP. In the electrode surface modified with AuNP-functionalized reduced graphene oxide (Au@rGO), hairpin probe HP1 and target DNA, ALP@DNAhg was captured through the hybridization of HP1 and another hairpin (HP2) overhung in DNAhg. Spontaneously tDNA was displaced and further unfolded HP1 and the presence of HP2 displaced tDNA to initiate repetitive recycling for signal amplification. When introducing $P_2O_7^{4-}$ and acidic MoO_4^{2-}, ALP catalyzed $P_2O_7^{4-}$ hydrolysis to produce PO_4^{3-}, in situ precipitating $PMo_{12}O_{40}^{3-}$ for signal readout. Importantly, with the excellent conductivity and nanosheet structure, Au@rGO as modifier was favorable to stabilize $PMo_{12}O_{40}^{3-}$ and promote electron transfer [19, 29]. This detection approach for tDNA would be highly sensitive, stable and cost-effective. It can open a new analytical route in disease diagnosis and molecular biology.

Experimental

Apparatus

A scanning electron microscope (SEM, S-4800, Hitachi, Japan, http://www.hitachi.com) was used to obtain scanning electron micrographs (SEM). The hybridization reaction of different DNA samples was investigated by polyacrylamide gel electrophoresis (PAGE), which was carried out on a Bio-Rad electrophoresis analyzer (Bio-Rad, USA, http://www.bio-rad.com). Cyclic voltammetry (CV), square wave voltammetry (SWV) and electrochemical impedance spectroscopy (EIS) were measured with a CHI660D electrochemical workstation (Shanghai Chenhua Instrument, China, http://www.chinstr.com). A three-electrode system included a modified glassy carbon electrode (GCE, $\Phi = 4$ mm), a saturated calomel electrode (SCE) and a platinum wire as working, reference and auxiliary electrode, respectively.

Chemicals and reagents

Nanjing Xianfeng Nano Co. (Nanjing, China, http://www.xfnano.com) offered us graphene oxide (GO). Chloroauric acid ($HAuCl_4 \cdot 4H_2O$), alkaline phosphatase (ALP), sodium pyrophosphate decahydrate ($Na_4P_2O_7 \cdot 2H_2O$), sodium molybdate dehydrate ($Na_2MoO_4 \cdot 2H_2O$), and 6-mercaptohexanol (MCH) were obtained from Sigma-Aldrich (St. Louis, MO, USA, http://www.sigmaaldrich.com). Terminal deoxynucleotidyl transferase (TdT) and TdT buffer (pH 7.2) containing 1 mM $CoCl_2$, 0.2 M potassium cacodylate, 0.2 mM DTT and 25 mM tris(hydroxymethyl) aminomethane (Tris) were provided by New England Biolabs, Inc. (USA, https://www.neb.com). All HPLC-purified oligonucleotides, deoxyadenosine triphosphate (dATP) and deoxythymidine triphosphate (dTTP) were purchased from Sangon Biotech Co., Ltd. (Shanghai, China, https://www.sangon.com). The stock solution of oligonucleotides was prepared with Tris-HCl buffer (pH 7.4) containing 1 mM $MgCl_2$, 1 mM $CaCl_2$, 5 mM KCl and 140 mM NaCl. Phosphate buffered saline (PBS, pH 7.0, 7.4) with 0.1 M NaH_2PO_4, 0.1 M Na_2HPO_4 and 2 mM $MgCl_2$ was used as working solution. In all experiments deionized water (DI water) (≥18.2 MΩ·cm, Milli-Q, Millipore, https://www.merckmillipore.com/CN/zh) was used. The detailed base sequences of all the oligonucleotides are listed in Table 1.

Target DNA (tDNA) with 26 bases is completely complementary to the underlined letters of the -SH-modified hairpin DNA (HP1). The bolded letters of HP1 are complementary each other to form the stem domain of hairpin structure. For the four DNA single strands (S1, S2, S3 and S4), the underlined- and double-underlined letters of S1 are complementary to those of S4 and S2. The dashed- and dotted-underlined letters of S3 are complementary to those of S2 and S4. The base sequences of S2 and S4 designated as

Table 1 Base sequence of all the oligonucleotides used in this work

Name	Sequence (5′ - 3′)
Target DNA (tDNA)	ATGGAGGACGTGTGCGGCCGCCTGGT
Hairpin DNA (HP1)	**TGTGCGG*CCGCCTGGT***ATGG ACATGGA***ACCAGGC GGCCGCACA** CGTCCTCCATAAA-SH
S1	CGCAATCC TGAGCACG
S2	***TGTGCGGCCGCCTGGTTCCATGTCCA TACCAGGCGG*** *AAGGAGCGACT* **(HP2)** CGTGCTCA CCGAATGC
S3	GCATTCGG ACTATGGC
S4	***TGTGCGGCCGCCTGGTTCCATGTCCA TACCAGGCGG****AAGGAGCGACT* **(HP2)** GCCATAGT GGATTGCG
One mismatch (M1)	ATGGAGGACGTGCGCGGCCGCCTGGT
Two mismatch (M2)	ATGGAGGACGTGCGCCGCCGCCTGGT
Three mismatch (M3)	ATGGAGGACGTGCCCCGCCGCCTGGT

italicized letters are to form a hairpin structure (HP2). The bolded letters of HP2 are complementary to those of HP1. As such, the equal stoichiometric S1, S2, S3 and S4 are designed to form an X-shape DNA (X-DNA) with two HP2 overhangs. Moreover, one-, two- and three-mismatched single strands (M1, M2 and M3) over tDNA are used to evaluate the biosensor specificity.

Preparation of AuNP-functionalized reduced graphene oxide (au@rGO)

Briefly, 10 mL of GO (0.5 mg·mL^{-1}) in DI water was mixed with 200 μL of $HAuCl_4$ (1%) and 20 μL of polyethylene glycol (PEG, 1%), and sonicated for 1 h [29]. The resulting solution in a Teflon-lined autoclave container was then maintained for 12 h at 180 °C. After cooling down to room temperature (RT), the black products Au@rGO were collected by centrifugation and washing at least three times, and finally redispersed in 1 mL DI water for further experiment. The SEM images of Au@rGO and rGO are displayed in Fig. S1 in the Electronic Supplementary Material).

Preparation of ALP-encapsulated DNA hydrogels (ALP@DNAhg)

According to previous method with a little modification [20], a mixture of 20 μL of S1, S2, S3 and S4 (2 μM) was heated to 30 °C for 30 min and cooled down to RT, allowing for the formation of X-DNA with HP2 overhangs. Then, 15 μL dATP/dTTP (50 mM) and 5 μL of TdT (20 U) were added. When incubated at 37 °C for 1 h, the formed X-DNA stretched in four directions to construct two X-DNA motifs with poly-A and poly-T tails (X-DNA-pAn and X-DNA-pTn). Upon addition of 10 μL ALP (1.0 mg mL^{-1}) for another 2 h, the final ALP@DNAhg polymers with HP2 overhangs were obtained and stored at 4 °C. Scheme 1a illustrated the preparation process.

Fabrication of the electrochemical biosensor

As shown in Scheme 1b, the bare glass carbon electrode (GCE, 4 mm in diameter) was pretreated by polishing with Al_2O_3 slurry (0.3 and 0.05 μm) and sonicating in anhydrous ethanol and DI water. Next, 10 μL of Au@rGO was added (Au@rGO/GCE), followed by the incubation of 10 μL HP1 (2 μM) annealed by heating to 90 °C for 10 min and cooling down to RT for 14 h (HP1/Au@rGO/GCE). After introducing 1 mM MCH as blocking reagent for 30 min (MCH/HP1/Au@rGO/GCE), 10 μL of tDNA standard solution with different concentrations was incubated for 2 h, allowing for the hybridization of unfolded HP1 with tDNA (tDNA/MCH/HP1/Au@rGO/GCE). Upon treatment with 10 μL ALP@DNAhg for another 1 h, tDNA displacement and recycling were initiated (ALP@DNAhg/tDNA/MCH/HP1/Au@ rGO/GCE). When adding 20 μL of $P_2O_7^{4-}$ and acidic MoO_4^{2-} (their ratio was optimized), the enwrapped ALP in DNAhg catalyzed $P_2O_7^{4-}$ hydrolysis to produce PO_4^{3-}, and simultaneously PO_4^{3-} combined with MoO_4^{2-} to in situ precipitate electroactive $PMo_{12}O_{40}^{3-}$ in the electrode surface. The response signal from $PMo_{12}O_{40}^{3-}$ was dependent on the tDNA concentration. It is noted that the modified electrode after each fabrication and before measurement was rinsed with DI water to avoid the physical absorption.

Electrochemical measurements

CV characterization of the biosensor was carried out in PBS (pH 7.4) containing 5 mM $[Fe(CN)_6]^{4-/3-}$ and 0.5 M H_2SO_4, respectively. EIS was carried out in PBS (pH 7.4) containing 5 mM $[Fe(CN)_6]^{4-/3-}$. CV curves were obtained in the potential range of −0.2 to 0.6 V at 100 mV·s^{-1} scan rate. SWV signals for the optimization of experiment conditions and the investigation of the analytical performance were tested in 0.5 M H_2SO_4 in the potential range of 0 to 0.4 V. EIS was measured in ac frequency range of 10^{-1} to 10^5 Hz with 5 mV excitation signal.

Results and discussion

Design of this electrochemical assay strategy

To obtain an X-DNA building block through DNA hybridization reaction, we especially designed four DNA single strands (S1, S2, S3 and S4) with complementary sequences. Among them, both S2 and S4 contained one same hairpin structure DNA (HP2) in their 5′-terminus. As such, one X-DNA containing two HP2 can recognize and hybridize with another hairpin DNA (HP1) immobilized in the electrode surface as capture probe. With the help of TdT, dATP and

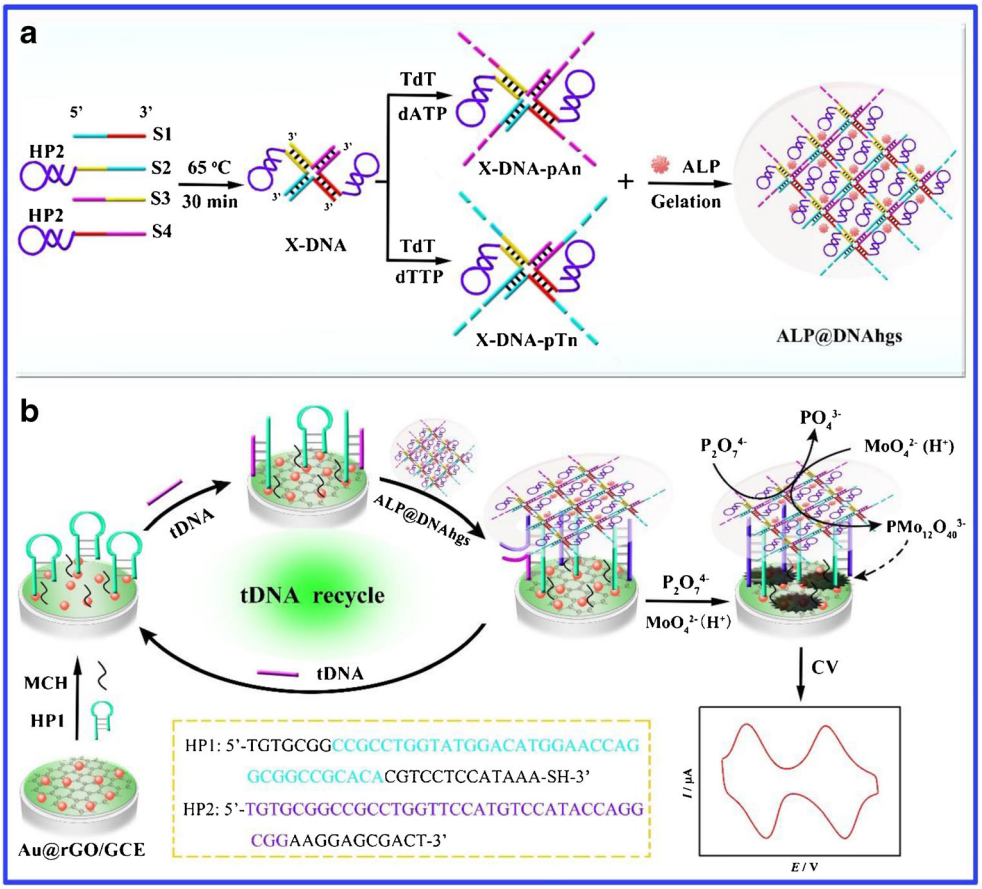

Scheme 1 Schematic illustration of (**a**) preparation of alkaline phosphatase- encapsulated DNA hydrogels (ALP@DNAhg), and (**b**) fabrication of the tDNA biosensor based on ALP@DNAhg to catalyze the in situ precipitation of electroactive $PMo_{12}O_{40}^{3-}$ anions with Keggin-structure, achieving tDNA-dependent electrochemical signal readout

dTTP, these formed X-DNA blocks with HP2 overhangs stretched in four directions for the assembly of X-DNA motifs with poly-A/T tails (X-DNA-pAn/pTn). Simultaneously they are polymerized into DNAhg with networked structure and good porosity, in which numerous ALP was enwrapped. The formation of ALP@DNAhg with many HP2 overhangs may be just like self-assembled DNAhg to encapsulate different enzymes or metal nanohybrids with catalytic activity [26]. Here, the unique performances of DNAhg facilitated the stable enwrapping of ALP, providing favorable accessibility to catalyze $P_2O_7^{4-}$ hydrolysis for the in situ production of PO_4^{3-}. In the electrode surface successively incubated with Au@rGO, HP1 and tDNA, the hybridization of HP1 and HP2 displaced tDNA and initiated tDNA recycling, resulting in the stable immobilization of ALP@DNAhg. When introducing $P_2O_7^{4-}$ and acidic MoO_4^{2-} (0.5 M H_2SO_4), electroactive $PMo_{12}O_{40}^{3-}$ was homogenously precipitated thanks to the chemical combination of MoO_4^{2-} and PO_4^{3-} from ALP-catalyzed $P_2O_7^{4-}$ hydrolysis. Moreover, the good conductivity and unique nanosheet structure of Au@rGO were desirable for the long-term stability of ALP@DNAhg and enhancing the electron transfer. Thus, highly sensitive, specific and cost-effective electrochemical assay of tDNA can be achieved.

Comparison of electrochemical signals in different situations

To demonstrate the electrochemical behavior of Au@rGO-modified electrode with $PMo_{12}O_{40}^{3-}$ precipitates, we investigated the CV response in the optimized experiment conditions (see Fig. S2 in the Electronic Supplementary Material). From Fig. 1a, no redox peak was observed for the modified electrode (ALP@DNAhg/tDNA/MCH/HP1/Au@rGO/GCE) in the absence of $P_2O_7^{4-}$ and acidic MoO_4^{2-} (curve a). When introducing $P_2O_7^{4-}$ and MoO_4^{2-}, significant CV response with two pairs of redox peaks at about 0.19 V and 0.37 V (curve b) were observed. This indicated that ALP-catalyzed $P_2O_7^{4-}$ hydrolysis greatly promoted the combination of PO_4^{3-} with MoO_4^{2-}, and the in situ precipitated $PMo_{12}O_{40}^{3-}$ served as redox mediator. The SEM images of $PMo_{12}O_{40}^{3-}$ precipitates was displayed in Fig. S1 in the Electronic Supplementary Material). Noticeably, the two peak currents of $PMo_{12}O_{40}^{3-}$ originates from two successive electron transfer processes that Mo atom undergoes, producing measurable electrochemical signal [30]. It is in good agreement with the reduction and oxidation of Keggin-structure α-$PMo_{12}O_{40}^{3-}$ anion through two- and four-electron processes in the reported literatures [12, 14, 30]. The $PMo_{12}O_{40}^{3-}$ formation (Eq. 1) and its electrochemical reaction (Eqs. 2 and 3) in the electrode surface can

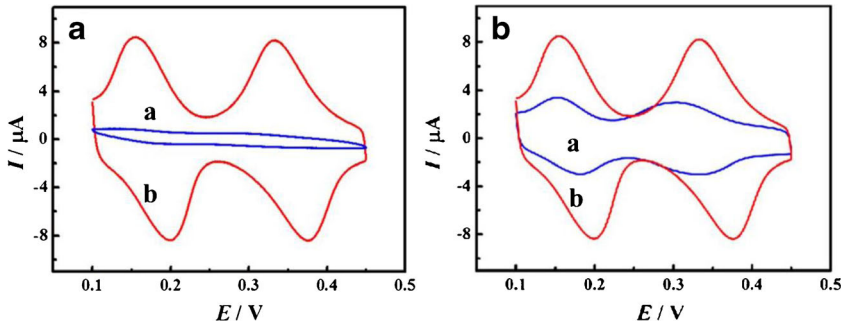

Fig. 1 CV response of (**a**) the Au@rGO-modified electrode (ALP@DNAhg/tDNA/ MCH/HP1/Au@rGO/GCE) before (curve a) and after (curve b) adding $P_2O_7^{4-}$ and acidic MoO_4^{2-} for in situ precipitation of electroactive $PMo_{12}O_{40}^{3-}$, and (**b**) the modified electrode without (curve a) and with (curve b) Au@rGO after adding $P_2O_7^{4-}$ and acidic MoO_4^{2-} for in situ precipitation of electroactive $PMo_{12}O_{40}^{3-}$. The CV responses were performed in 2 mL of 0.5 M H_2SO_4

be shown as follows:

$$12MoO_4^{2-} + 24H^+ + PO_4^{3-} = PMo_{12}O_{40}^{3-} + 12H_2O \quad (1)$$

$$PMo_{12}O_{40}^{3-} + 2e^- + 2H^+ = H_2PMo_2{}^{V}Mo_{10}{}^{VI}O_{40}^{3-} \quad (2)$$

$$H_2PMo_2{}^{V}Mo_{10}{}^{VI}O_{40}^{3-} + 2e^- + 2H^+ = H_4PMo_4{}^{V}Mo_8{}^{VI}O_{40}^{3-} \quad (3)$$

Moreover, Au@rGO with excellent conductivity and nanosheet structure were used as modifiers to increase the active electrode area and promote the electron transfer. The electroactive surface area of Au@rGO/GCE was investigated in Fig. S3 in the Electronic Supplementary Material. For the proof-of-concept, the CV response of $PMo_{12}O_{40}^{3-}$-precipitated electrode without and with Au@rGO modification was investigated. From Fig. 1b, compared with the Au@rGO-free electrode (curve a), about three times increasing of CV signal was observed for the Au@rGO-modified electrode (curve b). This suggested that Au@rGO greatly promoted the redox electron transfer of $PMo_{12}O_{40}^{3-}$ in the sensing interface and enhanced the stable immobilization of $PMo_{12}O_{40}^{3-}$ due to the strong chemisorption [19].

Electrochemical characterization

Based on ALP@DNAhg catalysis for in situ precipitation of redox $PMo_{12}O_{40}^{3-}$ and tDNA recycling amplification, the electrochemical strategy was developed for sensitive AD-related tDNA detection. The CV and EIS response of each fabrication step were measured in PBS (pH 7.4) containing 5 mM $[Fe(CN)_6]^{4-/3-}$. From Fig. 2a, b, bare GCE showed a well-defined redox peak in CV and a small semicircle in EIS (curve a). The modification of Au@rGO led to a sharply increased CV current and decreased electron transfer resistance (R_{et}) (curve b), attributing to the excellent conductivity of Au@rGO. Followed that, the sequential incubation of HP1, MCH, tDNA and ALP@DNAhg resulted in continuously decreased CV signal and increased R_{et} in EIS (curve c, d, e and f). This was ascribed to such a fact that the nonelectrical conductivity, steric hindrance and electrostatic repulsion to $[Fe(CN)_6]^{4-/3-}$ cooperatively hindered the electron transfer in the electrode interface.

Analytical performance

Under the optimized experiment conditions, the SWV signal of the biosensor in response to different concentrations of tDNA was measured in 0.5 M H_2SO_4 solution. As displayed in Fig. 3a, with the increasing of tDNA concentrations from 1.0×10^{-2} to 1.0×10^{4} pM, the SWV peak current corresponding to the peak voltage (i_p) 0.2 V was gradually increased. Fig. 3b showed a good linear relationship between the resultant peak

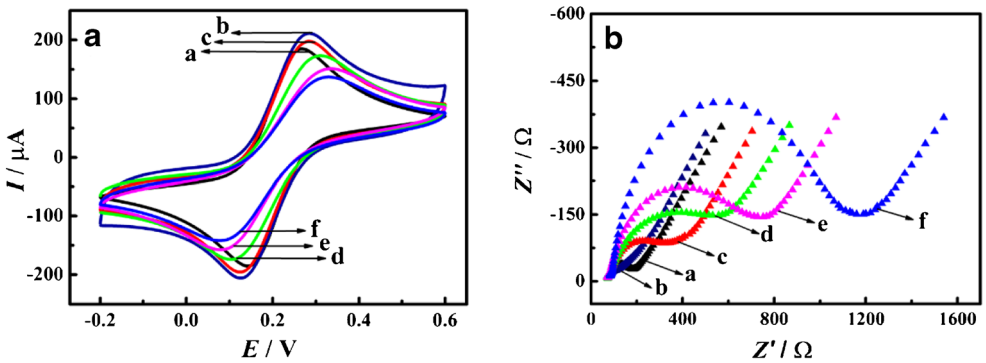

Fig. 2 CV curves (**a**) and EIS plots (**b**) of (a) GCE, (b) Au@rGO/GCE, (c) HP1/Au@rGO/GCE, (d) MCH/HP1/Au@rGO/GCE, (e) tDNA/MCH/HP1/Au@rGO/GCE, (f) ALP@DNAhg/tDNA/MCH/HP1/Au@rGO/GCE measured in PBS (pH 7.4) containing 5 mM $[Fe(CN)_6]^{4-/3-}$

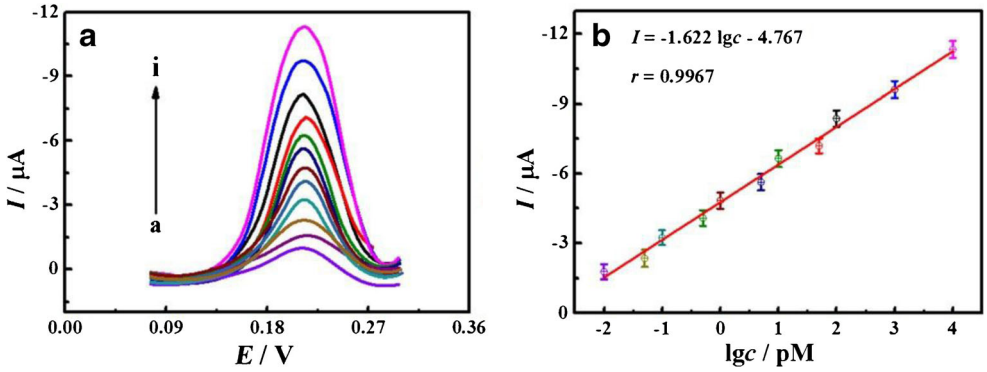

Fig. 3 **a** SWV responses of the electrochemical biosensor to tDNA in the range of 0, 1.0×10^{-2}, 5.0×10^{-2}, 0.10, 0.50, 1.0, 5.0, 10, 50, 1.0×10^{2}, 1.0×10^{3}, 1.0×10^{4} pM (from curve a to i) measured in 0.5 M H_2SO_4 under the optimized conditions. **b** The calibration relationship plotted by the resultant SWV peak current I (μA) at 0.2 V peak voltage vs. the logarithm of tDNA concentration (pM). Error bars: s, $n = 6$

current I (μA) at 0.2 V and the logarithm of tDNA concentration. The regression equation was I (μA) = $-1.622\lg c - 4.767$ with a correlation coefficient (r) of 0.9967. In terms of the rule of $3s_B/m$ [31, 32], the limit of detection (LOD) was obtained to be 3.4×10^{-3} pM. The high detection sensitivity and wide linear range may be attributed to three main concerns: (i) The networked-structure and integrated porosity of self-assembled DNAhg as favorable matrix provided great capability to encapsulate large amount of ALP, forming ALP@DNAhg with many HP2 overhangs. (ii) The hybridization of HP2 overhung in ALP@DNAhg with HP1 initiated the tDNA-recycling amplification and the stable immobilization of ALP. (iii) The catalysis capacity of ALP to $P_2O_7^{4-}$ hydrolysis enabled the in situ homogenous precipitation of redox $PMo_{12}O_{40}^{3-}$ for significantly amplified electrochemical current. Moreover, Au@rGO also enhanced the long-term orientation of $PMo_{12}O_{40}^{3-}$ and promoted electron transfer. As shown in Table 2, these advantageous features were comparable with or superior to those of various methodologies for DNA detection such as chemiluminescence, colorimetry, CV and differential pulse voltammetry.

Specificity, reproducibility and stability

The selectivity is crucial for the precise determination of analytes in real samples. We investigated the SWV response of three base-mismatched DNA sequences, one-base (M1, 10 nM), two-base (M2, 10 nM) and three-base (M3, 10 nM) as interferents against 1 nM tDNA. From Fig. 4a, the biosensor to tDNA showed significantly much higher SWV signal than the blank, M1, M2 and M3, although the tDNA concentration was lower 10 times than those of mismatched M1, M2 and M3, indicating acceptable specificity to tDNA.

Under the optimal conditions, five electrodes were prepared in one-batch and five-batch, respectively, and measured the SWV signal in 0.5 M H_2SO_4 solution. From Fig. 4b, the SWV peak currents showed a relative standard deviation (RSD) of 4.2% and 5.7% for intra- and inter-batch, respectively, indicating good precision in repeated electrochemical measurements.

Furthermore, after stored at 4 °C for 5, 10, 15 and 20 days, the corresponding SWV signals of the biosensor retained 96.2% – 84.5% of their initial response (Fig. 4c). The excellent stability may be originated from the strong

Table 2 Comparison of analytical performances of different methodologies for different target DNAs

Methods	Strategies	Target DNA (5′-3′)	Linear range	LOD	Ref.
Colorimetry	Disassembly of AuNP based on DNA displacement reaction	GCGACTTGACGTTA CCCCTTCGATCCTGTATA AA	0–40 nM	2 nM	[33]
CL	Catalysis of hemin/G- quadruplex to luminol-H_2O_2 system	GGAAGACTCTTGT	0.01–1.0 pM	8 fM	[34]
CV	EATR and guanine nanowire amplification	ACTGCTAGAGATTT TCCACAT	0.01–100 nM	3.6 pM	[35]
DPV	Catalysis of hemin/ G-quadruplex	GGAAGACTCTTGTCT	10–500 fM	10 fM	[36]
DPV	ALP and hemin/G- quadruplex-catalyzed oxidation of 1-naphthol	GGTTGGTGTGGTTGG	0.001–30 nM	0.37 pM	[37]
SWV	In situ generation of redox active $PMo_{12}O_{40}^{3-}$ catalyzed by ALP@DNAhg and tDNA recycling	ATGGAGGACGTGTG CGGCCGCCTGGT	1.0×10^{-2}-1.0×10^{4} pM	3.4 fM	this work

PDANTs: polydopamine-nanotubes, FAM: 6-carboxyfluorescein, EATR: Exo III-assisted target recycling

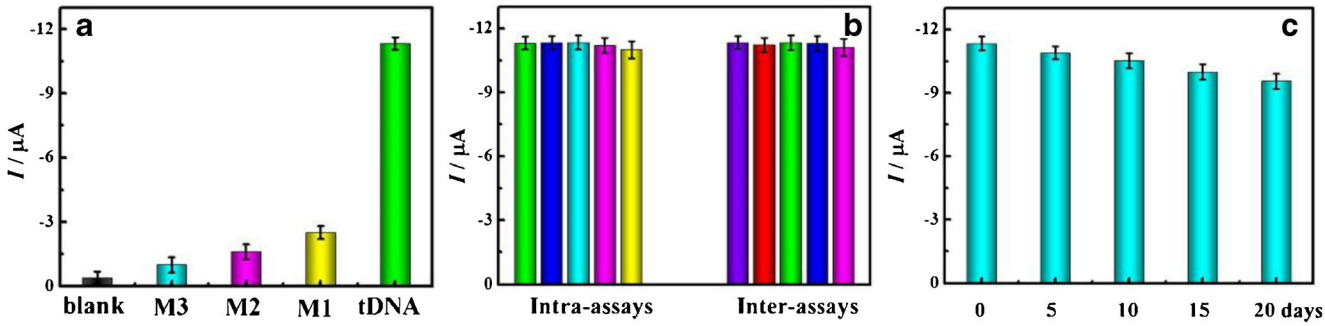

Fig. 4 **a** Specificity of the biosensor to M1 (10 nM), M2 (10 nM) and M3 (10 nM) against 1 nM tDNA. **b** Reproducibility and (**c**) stability of the biosensor. The tested solution for SWV signal was 0.5 M H_2SO_4. Error bars: *s*, $n = 6$

chemisorption and stable immobilization of $PMo_{12}O_{40}^{3-}$ in Au@rGO nanosheet structure.

Preliminary application

To validate the preliminary applicability of the biosensor in actual samples, the tDNA content in human serum sample that was obtained from the Xinqiao Hospital, the Army Medical University (Chongqing, China) was evaluated by using standard addition method. Prior to measuring SWV signal, the serum samples were diluted 10-fold with 0.1 M PBS (pH 7.4) and then tDNA standard solution of different concentrations was introduced for the incubation of biosensor. Under the optimum experiment conditions, the corresponding SWV response was measured in 0.5 M H_2SO_4 solution. As exhibited in Table S1, the tDNA recovery in the range of 98%–110% was obtained with RSD of 3.2%–6.5%, demonstrating the reliable and potential practicability in real biological samples.

Conclusions

An electrochemical biosensor was developed for the highly sensitive and selective detection of AD-related tDNA. This assay route was based on ALP-enwrapped DNA hydrogels (ALP@DNAhg) to catalyze the in situ homogenous precipitation of electroactive $PMo_{12}O_{40}^{3-}$ and tDNA recycling amplification. As such, our strategy shows unique and inherent features. (i) The integrated porosity and networked-structure of DNAhg facilitated the stable encapsulation of large amount of ALP. (ii) The further signal amplification was achieved by tDNA recycling initiated by strand displacement reaction, enabling more stable immobilization of ALP than specific biotin-SA combination [18] and efficient catalysis to $P_2O_7^{2-}$ hydrolysis for producing PO_4^{3-}. (iii) The nanosheet structure and excellent conductivity of Au@rGO as modifiers were favorable for the long-term orientation and promoting electron transfer of $PMo_{12}O_{40}^{3-}$. It should be noted that the catalysis substrate $P_2O_7^{2-}$ of ALP is more superior and more cost-effective than organic NPP, and the hydrolysis product of $P_2O_7^{2-}$ is simpler than that of NPP [18]. Maybe, the condition of preparing ALP@DNAhg sometimes is difficultly controlled, resulting in relatively low reproducibility and long-term stability. From this point of view, the applicability of our method in some practical samples may be limited. In the future, we would attempt to do many in-depth works to improve the features of DNA hydrogels and the electrochemical assay platforms.

Acknowledgements The financial support by the National Natural Science Foundation (NNSF) of China (21775123) and the Natural Science Foundation Project of Chongqing (cstc2018jcyjAX0214) to this work was deeply appreciated.

Compliance with ethical standards The author(s) declare that they have no competing interests.

References

1. Su S, Sun HF, Cao WF, Chao J, Peng HZ, Zuo XL, Yuwen LH, Fan CH, Wang LH (2016) Dual-target electrochemical biosensing based on DNA structural switching on gold nanoparticle-decorated MoS_2 nanosheets. ACS Appl Mater Interfaces 8:6826–6833
2. Cui L, Lu MF, Li Y, Tang B, Zhang CY (2018) A reusable ratiometric electrochemical biosensor on the basis of the binding of methylene blue to DNA with alternating AT base sequence for sensitive detection of adenosine. Biosens Bioelectron 102:87–93
3. Zhao J, Gao J, Zheng T, Yang Z, Chai Y, Chen S, Yuan R, Xu W (2018) Highly sensitive electrochemical assay for Nosema bombycis gene DNA PTP1 via conformational switch of DNA nanostructures regulated by H^+ from LAMP. Biosens Bioelectron 106:186–192
4. Zheng TT, Zhang QF, Feng S, Zhu JJ, Wang Q, Wang H (2014) Robust nonenzymatic hybrid nanoelectrocatalysts for signal amplification toward ultrasensitive electrochemical cytosensing. J Am Chem Soc 136:2288–2291
5. Ngo TA, Nakata E, Saimura M, Morii T (2016) Spatially organized enzymes drive cofactor-coupled cascade reactions. J Am Chem Soc 138:3012–3021
6. Lv YQ, Chen SY, Shen YF, Ji JJ, Zhou Q, Liu SQ, Zhang YJ (2018) Competitive multiple-mechanism-driven electrochemiluminescent

detection of 8-hydroxy-2′-deoxyguanosine. J Am Chem Soc 140: 2801–2804
7. Wu YM, Xu WJ, Bai LJ, Yuan YL, Yi HY, Chai YQ, Yuan R (2013) Ultrasensitive thrombin detection based on direct electrochemistry of highly loaded hemoglobin spheres-encapsulated platinum nanoparticles as labels and electrocatalysts. Biosens Bioelectron 50:50–56
8. Xu MD, Zhuang JY, Chen X, Chen GN, Tang DP (2013) A difunctional DNA–AuNP dendrimer coupling DNAzyme with intercalators for femtomolar detection of nucleic acids. Chem Commun 49:7304–7306
9. Liu TZ, Hu R, Zhang X, Zhang KL, Liu Y, Zhang XB, Bai RY, Li DL, Yang YH (2016) Metal–organic framework nanomaterials as novel signal probes for electron transfer mediated ultrasensitive electrochemical immunoassay. Anal Chem 88:12516–12523
10. Li JY, Si L, Bao JC, Wang ZY, Dai ZH (2017) Fluorescence regulation of poly(thymine)-templated copper nanoparticles via an enzyme-triggered reaction toward sensitive and selective detection of alkaline phosphatase. Anal Chem 89:3681–3686
11. Si Z, Xie B, Cahen Z, Tang C, Li T, Yang M (2017) Electrochemical aptasensor for the cancer biomarker CEA based on aptamer induced current due to formation of molybdophosphate. Microchim Acta 184:3215–3221
12. Sadakane M, Steckhan E (1998) Electrochemical properties of polyoxometalates as electrocatalysts. Chem Rev 98:219–237
13. Huang YX, Tang C, Liu J, Cheng J, Si ZZ, Li T, Yang MH (2017) Signal amplification strategy for electrochemical immunosensing based on a molybdophosphate induced enhanced redox current on the surface of hydroxyapatite nanoparticles. Microchim Acta 184: 855–861
14. Qu FL, Yang MH, Rasooly A (2016) Dual signal amplification electrochemical biosensor for monitoring the activity and inhibition of the Alzheimer's related protease β-secretase. Anal Chem 88: 10559–10565
15. Hu LS, Hu SQ, Guo LY, Shen CC, Yang MH, Rasooly A (2017) DNA generated electric current biosensor. Anal Chem 89:2547–2552
16. Feng KJ, Liu J, Deng L, Yu HJ, Yang MH (2018) Amperometric detection of microRNA based on DNA-controlled current of a molybdophosphate redox probe and amplification via hybridization chain reaction. Microchim Acta 185:28
17. Xie SB, Yuan YL, Chai YQ, Yuan R (2015) Tracing phosphate ions generated during loop-mediated isothermal amplification for electrochemical detection of Nosema bombycis genomic DNA PTP1. Anal Chem 87:10268–10274
18. Cai W, Xie SB, Tang Y, Chai YQ, Yuan R, Zhang J (2017) A label-free electrochemical biosensor for microRNA detection based on catalytic hairpin assembly and in situ formation of molybdophosphate. Talanta 163:65–71
19. Shen CC, Li XZ, Rasooly A, Guo LY, Zhang K, Yang MH (2016) A single electrochemical biosensor for detecting the activity and inhibition of both protein kinase and alkaline phosphatase based on phosphate ions induced deposition of redox precipitates. Biosens Bioelectron 85:220–225
20. He Y, Yang X, Yuan R, Chai YQ (2017) Switchable target-responsive 3D DNA hydrogels as a signal amplification strategy combining with SERS technique for ultrasensitive detection of miRNA 155. Anal Chem 89:8538–8544
21. Lilienthal SV, Shpilt ZH, Wang F, Orbach R, Willner I (2015) Programmed DNAzyme-triggered dissolution of DNA-based hydrogels: means for controlled release of biocatalysts and for the activation of enzyme cascades. ACS Appl Mater Interfaces 7:8923–8931
22. Li J, Zheng C, Cansiz S, Wu CC, Xu JH, Cui C, Liu Y, Hou WJ, Wang YY, Zhang LQ, Teng IT, Yang HH, Tan WH (2015) Self-assembly of DNA nanohydrogels with controllable size and stimuli-responsive property for targeted gene regulation therapy. J Am Chem Soc 137:1412–1415
23. Li J, Mo LT, Lu CH, Fu T, Yang HH, Tan WH (2016) Functional nucleic acid-based hydrogels for bioanalytical and biomedical applications. Chem Soc Rev 45:1410
24. Zhou L, Sun N, Xu LJ, Chen X, Cheng H, Wang J, Pei RJ (2016) Dual signal amplification by an "on-command" pure DNA hydrogel encapsulating HRP for colorimetric detection of ochratoxin A. RSC Adv 6:114500–114504
25. Zhu XL, Mao XX, Wang ZH, Feng C, Chen GF, Li GX (2017) Fabrication of nanozyme@ DNA hydrogel and its application in biomedical analysis. Nano Res 10:959–970
26. Mao XX, Chen GF, Wang ZH, Zhang YG, Zhu XL, Li GX (2018) Surface-immobilized and self-shaped DNA hydrogels and their application in biosensing. Chem Sci 9:811–818
27. Zhu Z, Guan Z, Jia S, Lei Z, Lin S, Zhang H, Ma Y, Tian ZQ, Yang CJ (2014) Au@ Pt nanoparticle encapsulated target-responsive hydrogel with volumetric bar-chart chip readout for quantitative point-of-care testing. Angew Chem Int Ed 53:12503–12507
28. Liu SF, Wang CF, Zhang CX, Wang Y, Tang B (2013) Label-free and ultrasensitive electrochemical detection of nucleic acids based on autocatalytic and exonuclease III-assisted target recycling strategy. Anal Chem 85:2282–2288
29. Wu XY, Chai YQ, Zhang P, Yuan R (2015) An electrochemical biosensor for sensitive detection of microRNA-155: combining target recycling with cascade catalysis for signal amplification. ACS Appl Mater Interfaces 7:713–720
30. Shen CC, Zeng K, Luo JJ, Li XQ, Yang MH, Rasooly A (2017) Self-assembled DNA generated electric current biosensor for HER2 analysis. Anal Chem 89:10264–10269
31. Long GL, Winefordner JD (1983) Limit of detection. A closer look at the IUPAC definition. Anal Chem 55:712A–724A
32. Radi AE, Sanchez GLA, Baldrich E, O'Sullivan CK (2006) Reagentless, reusable, ultrasensitive electrochemical molecular beacon aptasensor. J Am Chem Soc 28:117–124
33. Zhou ZX, Wei W, Zhang YJ, Liu SQ (2013) DNA-responsive disassembly of AuNP aggregates: influence of nonbase-paired regions and colorimetric DNA detection by exonuclease III aided amplification. J Mater Chem B 1:2851–2858
34. Gao Y, Li BX (2014) Exonuclease III-assisted cascade signal amplification strategy for label-free and ultrasensitive chemiluminescence detection of DNA. Anal Chem 86:8881–8887
35. Huang YL, Gao ZF, Luo HQ, Li NB (2017) Sensitive detection of HIV gene by coupling exonuclease III-assisted target recycling and guanine nanowire amplification. Sens Actuators B Chem 238: 1017–1023
36. Liu CC, Kanekiyo T, Xu HX, Bu GJ (2013) Apolipoprotein E and Alzheimer disease: risk, mechanisms and therapy. Nat Rev Neurol 9:106–118
37. Yang ZH, Zhuo Y, Yuan R, Chai YQ (2015) Amplified thrombin aptasensor based on alkaline phosphatase and hemin/G-quadruplex-catalyzed oxidation of 1-naphthol. ACS Appl Mater Interfaces 7:10308–10315